

**Hot and Cold Spots
in the First plus Second Year COBE/DMR Maps**

L. Cayón and G. Smoot

Lawrence Berkeley Laboratory and Center for Particle Astrophysics, University of
California, Berkeley, CA 94720

Received _____; accepted _____

ABSTRACT

Matter density perturbations at the decoupling epoch produce angular fluctuations in the temperature of the Cosmic Microwave Background (CMB) radiation that may be observed as hot and cold spots. As observational data of the CMB includes instrumental noise in addition to the cosmological signal, one would like to determine which of the observed spots are produced by the noise and which ones correspond to signal. In this work we first present a statistical analysis of the first plus second year COBE/DMR map at 53 GHz that reveals the presence of cosmological signal in the data. The analysis is based on Harrison-Zeldovich Monte Carlo realizations and utilizes a generalized χ^2 statistic. The method is applied to the number of spots and the fraction of the total area that appear above/below a certain value of the dispersion of the noise, including and excluding the quadrupole, giving $Q_{rms-PS} = 15_{-6}^{+3}$, $18_{-7}^{+5}\mu K$ and $Q_{rms-PS} = 18_{-4}^{+3}$, $21 \pm 6\mu K$, at the 95% confidence level, respectively. The data taken by the COBE/DMR experiment during the first two years at three different frequencies (31, 53 and 90 GHz) are used to determine which of the spots observed at 53 GHz appear simultaneously in the other two channels. Six cold and eleven hot spots were found in coincidence in the three maps below and above the dispersion of the noise. The significance of those spots is calculated by comparison of their area and signal-to-noise with noise Monte Carlo simulations. We point out two cold spots and one hot spot at positions $(l, b) \approx (85^\circ, 40^\circ), (-21^\circ, -45^\circ), (-81^\circ, -33^\circ)$ respectively, at the 99% confidence level.

Subject headings: cosmic microwave background: data analysis

1. Introduction

Temperature fluctuations of the CMB radiation at large angular scales are directly related to the matter density fluctuations at last scattering surface (Sachs and Wolfe 1967). Direct observation of those fluctuations gives information on the seeds of the structures observed in the present Universe. Statistical analysis of the temperature of the CMB observed by the COBE/DMR experiment during 1990 revealed for the first time the presence of anisotropies (Smoot et al. 1992). Analysis of the COBE/DMR first year and first plus second years data have been performed by using different techniques. Techniques based on the correlation function (Smoot et al. 1992, Scaramella and Vittorio 1993, Seljak and Bertschinger 1993, Bennett et al. 1994), on orthogonal functions on a sphere with the galactic plane removed (Wright et al. 1994b, Gorski et al. 1994), on RMS estimations (Smoot et al. 1994, Banday et al. 1994) and on the topology of the maps (Smoot et al. 1994, Torres 1994a,b, Torres et al. 1994) revealed the presence of signal in the analysed data and showed the degeneracy in between the amplitude Q_{rms-PS} and the index n of the power spectrum of matter density fluctuations (higher values of n require lower values of Q_{rms-PS}).

Since the announcement of the detection anisotropies in the CMB temperature field by the COBE/DMR experiment, other experiments at different angular scales have also statistically detected CMB anisotropies in their data (see references in White, Scott and Silk 1994). Comparison of different experiments is required to confirm such detection. Ganga et al. 1993 found a strong correlation between the 170 GHz partial sky survey by FIRS experiment and the COBE/DMR first year data, indicating that the fluctuations observed by both experiments should correspond to the same anisotropies of the CMB. The detection of individual features in the data sets open new possibilities for comparison the observations of different experiments. The first experiment for which the detection of

those individual, primordial features has been claimed is the Tenerife experiment (Hancock et al. 1994). Possible contamination of the anisotropies observed by the COBE/DMR experiment has been studied regarding systematic effects (Kogut et al. 1992), Galactic and extragalactic foregrounds (Bennett et al. 1992, 1993) and magnitude of the noise correlation (Lineweaver et al. 1994). Although none of these effects are significant, the detection of individual structures requires special care in relation to the level of noise present in the maps at different frequencies.

The idea of this work is first, to confirm the presence of cosmological signal in the first plus second year COBE/DMR data by using characteristics of the features that appear in the maps, and second, to determine the significance of the hot and cold spots as compared with noise. A description of the analysed data can be found in section 2. Statistical analysis of the 53 GHz map is presented in section 3; the method is explained in subsection 3.1 and the results are given in subsection 3.2. In subsection 4.1 we show the method used to estimate the significance of the observed spots as compared with noise and the results are showed in subsection 4.2. A summary of the main conclusions is given in section 5.

2. Description of the Data

COBE/DMR produced CMB temperature sky maps at three frequencies 31, 53 and 90 GHz. Observations are made by two different channels A and B at each frequency. Data of the two channels were combined in a sum $(A + B)/2$ and a difference $(A - B)/2$ maps. The former is a combination of CMB signal and instrumental noise while the later contains only noise.

We analyse the first and second year data taken by the COBE/DMR experiment during 1990-1991. The analyzed maps ($(A + B)/2$ maps at different frequencies) have monopole and dipole (and optionally quadrupole) subtracted and a galactic cut of $|b| > 20^\circ$

is carried out. In order to improve the signal-to-noise ratio (ratio of the dispersion of the temperature of the $(A + B)/2$ map over the dispersion of the difference map, $RMS_{(A+B)/2}/RMS_{(A-B)/2}$) a gaussian smoothing of $FWHM = 7^\circ$ is performed, resulting in values of the signal-to-noise ratio of 1.1, 1.4 and 1.13 for the 31, 53 and 90 GHz data respectively. We search for connected pixels (spots) above and below several thresholds ν . The threshold is defined so that pixels above/below this level would have a temperature greater/lower or equal $\nu \times RMS_{(A-B)/2}$. Figures 1a and 1b show the spots found at the 3 frequencies above/below levels 1/-1 and 2/-2 respectively. At level 1 (figure 1a), six cold and eleven hot spots can be simultaneously observed at the three frequencies. These are the spots that are considered in section 4 to estimate the significance of the spots as compare with noise.

3. Statistical Analysis

3.1. Method

The purpose of this section is to set constraints on the amplitude of the power spectrum of the matter density fluctuations assuming a Harrison-Zeldovich power spectrum. We analyze the first plus second year data observed by the COBE/DMR experiment at 53 GHz as this is the channel with the lowest level of noise.

This analysis is based on Monte Carlo simulations made following the configuration of the DMR experiment. We simulate the CMB sky as seen by the DMR (beam filter given in Wright et al. 1994a) and create two maps, one including the noise of channel A and the other one including the noise of channel B . After that, the sum and difference maps are created. Mean and dipole subtraction, galactic cut and smoothing are performed as indicated in previous section (quadrupole subtraction is also performed to compare results including and non including it).

We use a generalized χ^2 statistic to determine the models favoured by the COBE/DMR data, considering the number of spots that appear at different thresholds and the fraction of the total area covered by them, FA . This method has been previously used by Torres et al. 1994 to set constraints on the amplitude of the power spectrum and the spectral index by analysing the genus in the first year COBE/DMR maps. The generalized χ^2 for each realization k is given by:

$$\chi_k^2 = \sum_{i=1}^{n_l} \sum_{j=1}^{n_l} (N_s^k(\nu_i) - N_s^d(\nu_i)) M_{ij}^{-1} (N_s^k(\nu_j) - N_s^d(\nu_j)) , \quad (1)$$

where n_l is the number of thresholds (ν) considered, $N_s^k(\nu_i)$ refers to the number of spots that appear at level ν_i in the k realization and $N_s^d(\nu_i)$ is the number of spots found in the data at ν_i . M_{ij} is the covariance matrix defined by:

$$M_{ij} = \left(\frac{1}{n_r} \sum_{k=1}^{n_r} (N_s^k(\nu_i) - \langle N_s(\nu_i) \rangle) (N_s^k(\nu_j) - \langle N_s(\nu_j) \rangle) \right) , \quad (2)$$

where n_r is the number of realizations, $n_r = 1000$ and the brackets represent the mean value averaging over the realizations. The χ^2 for the fraction of the area occupied by the spots is defined in the same way by substituting N_s by FA . We test models with values of the amplitude $Q_{rms-PS} = 0, 6, 9, 12, 15, 18, 21, 24, 27, 30$. In figure 2, we present an example of the distribution of χ^2 for three different models, calculated for the number of spots. As one can see from this figure, there is a significant statistical difference between different values of Q_{rms-PS} . For each of those models we first determine the mean value of the χ^2 obtained by comparing with the COBE/DMR data, averaged over 1000 realizations, and select the model with the minimum value. The error bars associated to that model are calculated by assuming that each of the realizations of that model are now the data and repeating the process.

3.2. Results

The application of the method explained above to the number of spots that can be seen in a map at different thresholds as compared with the ones observed in the first plus second year 53 GHz map gave a constrain on the amplitude of the power spectrum of $Q_{rms-PS} = 15_{-6}^{+3} \mu K$ at the 95% confidence level, assuming Harrison-Zeldovich. By applying the same technique to the FA we got $Q_{rms-PS} = 18_{-4}^{+3} \mu K$, at the same confidence level. The same analysis is performed excluding the quadrupole, giving $18_{-7}^{+5} \mu K$ for the number of spots and $21 \pm 6 \mu K$ for the fractional area, at the 95% confidence level. As it would be expected, the Q_{rms-PS} values grow when the quadrupole is subtracted. The intervals do not exclude each other and which is more important, the result confirms the presence of signal in the analyzed map of the two years of observations. Therefore, our purpose in next section is to estimate which of the spots that are observed in the maps have the lowest probability of being produced by noise and thus are likely real signal.

4. Significance of the Spots

4.1. Method

The aim of this section is to determine the significance of the spots present in the COBE/DMR maps in comparison with noise. For this purpose we study the distribution of several descriptors of spots in noise realizations and compare them with the corresponding values for the spots found in the data maps. The presence of the analysed spots in the data observed at the three frequencies is required. Once the spots found simultaneously in the three maps are selected, we concentrate in the 53 GHz map as it is the one with the highest signal-to-noise ratio.

Noise realizations are made following the specifications indicated in subsection 3.1. We first estimate the number of coincidences (number of spots observed simultaneously at the three frequencies) that can be produced by noise and compare with the real data. From 1000 realizations of pure noise the expected number of spots found in coincidence in the three frequencies below/above threshold $-1/1$ is ~ 4 . We find six cold and eleven hot spots in coincidence in the data taken at the three frequencies, 31, 53 and 90 GHz. Therefore, the data that we are analysing present some spots for which a non-noise origin could be attributed.

Once the spots are selected above different thresholds in the data maps as well as in the simulated maps (resulting from realizations performed in the way indicated in previous section) we determine the position of the barycenter (galactic coordinates) and calculate the area A and the signal-to-noise ratio S/N (as we will see, the S/N defined for the spots should not be confused with the signal-to-noise defined for the map in previous section). The area is defined by the number of connected pixels, where each pixel has a size of $2^\circ.6 \times 2^\circ.6$. The signal-to-noise ratio of the spot is given by the average of the signal-to-noise ratio of the connected pixels inside the spot n_c , that is, by the average of the ratio of the temperature T_i over the ratio of the channel dependent instrument noise dispersion per observation σ_s over the square root of the number of observations taken in each pixel N_i ,

$$S/N \equiv \frac{1}{n_c} \left| \sum_{i=1}^{n_c} \frac{T_i}{\frac{\sigma_s}{\sqrt{N_i}}} \right|. \quad (3)$$

We perform 1000 noise realizations (including the noise from the 53 GHz radiometer) and calculate the distribution of the characteristics defined above. Seventeen thresholds, in between -4 and 4 , are analysed. Comparison of the values found for each individual spot seen simultaneously in the three data maps at a fixed threshold with the noise error bars will give the significance level of them, as it is presented in the following subsection.

4.2. Results

At level 1 there are six cold and eleven hot spots that are simultaneously observed at the three frequencies, 31, 53 and 90 GHz. As it was indicated above, those are the spots that have been considered in this analysis. Tables 1.a and 1.b present the characteristics of the common spots as they appear in the 53 GHz map. The position of the barycenter is given in galactic coordinates (degrees) in the first two columns. Third and fifth columns give the area and the S/N of the spots. The probability of having spots produced by noise with area (S/N) lower or equal the area (S/N) of the observed spots is given in the fourth (sixth) column. The probability distribution function of the area and of the S/N can be seen in figures 3.a and 3.b respectively. The highest level at which the spot is observed is given in the seventh column of tables 1.a and 1.b. The mean value of the area that the spots occupy at the highest/lowest threshold at which they are observed is of approximately eight pixels ($\sim 7^\circ$ in extension), that is $\sim 700h^{-1}$ Mpc.

As can be seen from the tables, at $\nu = 1$, two cold spots at positions $(l, b) = (85^\circ, 40^\circ)$, $(-21^\circ, -45^\circ)$ and one hot spot at $(l, b) = (-81^\circ, -33^\circ)$ have a probability lower than 1% of being produced by noise as the values of the area and the signal-to-noise indicate. If we also include spots for which the probability of being produced by signal is bigger than $\sim 90\%$ considering the area and the signal-to-noise, we have two more cold spots (first and fourth spots) and three more hot spots (spots 2,7 and 8).

5. Conclusions

The presence of cosmological signal in the data observed during the first two years by the COBE/DMR experiment have been analyzed considering the characteristics of the features that appear in the maps. We performed a statistical analysis based on Monte Carlo

simulations of a Harrison Zeldovich power spectrum to set constraints on the amplitude of the power spectrum. A χ^2 statistic was calculated to compare the number of spots and the fraction of the area occupied by them assuming different models, with the first plus second year COBE/DMR data. From the number of spots we got, at the 95% confidence level, $Q_{rms-PS} = 15_{-6}^{+3}$, $18_{-7}^{+5}\mu K$ and from the fractional area $Q_{rms-PS} = 18_{-4}^{+3}$, $21 \pm 6\mu K$, including and non including the quadrupole. There have been previous analysis of the first year of data of the COBE/DMR experiment based on the characteristics of the features observed at different thresholds (Smoot et al. 1994, Torres 1994a,b, Torres et al. 1994). They got values of Q_{rms-PS} , with the spectral index forced to unity, which are inside the error bars that result from our analysis. The *RMS* of the first plus second year COBE/DMR data has been calculated by Banday et al. 1994. The 1σ intervals of the Q_{rms-PS} , subtracting and non subtracting the quadrupole, overlap with our results.

We have also determined the significance level of the hot and cold spots present in the first plus second year COBE/DMR maps as compared with noise. We used an statistical method based on Monte Carlo realizations of pure noise. The descriptors of the spots used for that analysis are the area and the signal-to-noise ratio. The presence of the spots in the three maps (at the three different frequencies) was required.

Eleven hot and six cold spots are found in coincidence in the three maps above and below threshold $1/ - 1$ respectively (only four cold and four hot spots would be expected to be produced by pure noise). From these spots we select two cold $((l, b) \approx (85^\circ, 40^\circ), (-21^\circ, -45^\circ))$ and one hot spot $((l, b) \approx (-81^\circ, -33^\circ))$ that have a probability of having a cosmological origin greater or equal the 99% when the area and the signal-to-noise are compared with pure noise.

The second hot spot that appears in table 1b has an area which has nearly a 100% probability of not being noise and a signal to noise ratio that is outside the 90% noise error

bars. This spot is situated above the Galactic center on the Ophiuchus loop which is a known feature of Galactic structure. Therefore that spot is very likely contaminated by the galactic emission that could still be affecting the analysed maps. The fact that its intensity decreases with the frequency is another indication of its probably galactic origin (although the spot has a higher intensity in the 53 GHz map than in the 31 GHz data however the level of noise at 31 GHz is bigger than at 53 GHz).

An analysis of the spots observed in the first year COBE/DMR data is presented in Torres 1994b. The level at which the spots are observed, as well as the area and the eccentricity are calculated. All those spots can also be seen in our data. In that previous paper there is no estimation of the noise contribution to the individual spots and the main conclusion is the compatibility of the data with a Harrison-Zeldovich spectrum with amplitude $Q = 16 \mu K$. The Wiener filter technique has been applied by Bunn et al. 1994 to the "Reduced galaxy" linear combination of the first year COBE/DMR sky maps. This technique requires the assumption of a certain power spectrum of the matter density fluctuations. Assuming a spectral index $n = 1.0$ and the corresponding spectral amplitude (Seljack and Bertschinger 1993) they performed constrained realizations of the CMB anisotropy. They observe two hot spots $(l, b) = (-85^\circ, -36^\circ), (55^\circ, 65^\circ)$ and a large cold spot at $(l, b) = (-100^\circ, 50^\circ)$ that appear highly significant in the simulated maps. All those spots are considered in our analysis as they appear in coincidence in the 31, 53 and 90 GHz two years maps. As indicated above, the hot spot located at $(l, b) = (55^\circ, 65^\circ)$ is very likely produced by the galaxy (the "Reduced Galaxy" map used by Bunn et al. 1994 can still have galactic contamination). The other hot spot is one of the spots pointed out in this work. The large cold spot observed at $(l, b) = (-100^\circ, 50^\circ)$ corresponds to the first one in table 1a. This spot has probability of having a cosmological origin greater than 95% as indicated by our analysis.

Up to now, comparison between results from different experiments has been performed

by statistical analysis of the observed fluctuations. Confirmation of those results can now be done by observation of the individual spots detected by the different experiments. Moreover, the presence of a hot/cold region detected by an experiment can be used to get information about the characteristics of the perturbations observed at the decoupling epoch by analysis of that region by other experiments. The analysis of the four years of COBE/DMR data will improve the significance of the results.

We acknowledge the excellent work of those contributing to the COBE/DMR. We would also like to thank A. Banday, A. Kogut, C. Lineweaver, E. Martínez-González, and L. Tenorio for helpful discussions. This work was supported in part at LBL through DOE Contract DOE-AC-03-76SF0098. L.C. acknowledges the support of a MEC/Fulbright fellowship (FU93 13924591). COBE is supported by the Office of Space Sciences of NASA Headquarters.

$l(^{\circ})$	$b(^{\circ})$	A	$P(A)\%$	S/N	$P(S/N)\%$	ν_{max}
-99	57	259	100	1.97	96	-4.0
85	40	82	99	2.23	99	-2.5
-21	-45	162	99	2.50	99	-3.5
73	-29	35	92	2.30	99	-3.5
81.5	-59	127	99	1.66	77	-2.0
-86	33	9	42	1.44	46	-1.0

Table 1a: Spots found below threshold -1 in the 53 GHz map, that appear simultaneously in the three DMR maps, at 31, 53 and 90 GHz. First two columns give the position of the barycenter in galactic coordinates, l, b in degrees. The third column shows the area, A , of the spots and the fourth column indicates the probability of finding spots created by pure noise with area smaller than the area of the spot found in the data, $p(A)$. The signal-to-noise of the spots, S/N is given in column five and the probability of having spots created by noise with S/N smaller than the signal-to-noise of the data is given in column six. Column seven shows the highest level at which the spots are observed.

$l(^{\circ})$	$b(^{\circ})$	A	$P(A)\%$	S/N	$P(S/N)\%$	ν_{max}
-24	51	29	87	1.86	92	2.5
41	71	375	100	1.99	97	4.0
12.5	-24	10	44	1.88	93	2.0
46	-32	53	97	1.65	76	2.5
96	-28	27	86	1.88	93	2.5
120	-36.6	56	97	1.70	81	2.5
176	-42	100	99	1.91	94	3.0
172	29	33	90	2.25	99	3.0
-81	-33	105	99	2.40	99	3.0
141	-73.5	69	98	1.56	64	2.0
-82	-58	8	36	2.08	99	1.0

Table 1b: Spots found above threshold 1 in the 53 GHz map, that appear simultaneously in the three DMR maps, at 31, 53 and 90 GHz. First two columns give the position of the barycenter in galactic coordinates, l, b in degrees. The third column shows the area, A , of the spots and the fourth column indicates the probability of finding spots created by pure noise with area smaller than the area of the spot found in the data, $p(A)$. The signal-to-noise of the spots, S/N is given in column five and the probability of having spots created by noise with S/N smaller than the signal-to-noise of the data is given in column six. Column seven shows the highest level at which the spots are observed.

REFERENCES

- Banday, A.J. et al. 1994, preprint
- Bennett, C.L. et al. 1992, ApJ, 391, 446
- Bennett, C.L. et al. 1993, ApJ, 414, L77
- Bennett, C.L. et al. 1994, ApJ, 436, in press
- Bunn, E.F., Fisher, K.B., Yehuda, H., Lahav, O., Silk, J. and Zaroubi, S. 1994, submitted to ApJ
- Ganga, K., Cheng, E., Meyer, S. & Page, L. 1993, ApJ, 410, L57
- Gorski, K. et al. 1994, ApJ, 430, L89
- Hancock, S., Davies, R.D., Lasenby, A.N., Gutiérrez de la Cruz, C.M., Watson, R.A., Rebolo, R. & Beckman, J.E. 1994, Nature, 367, 333
- Kogut, A. et al. 1992, ApJ, 401, 1
- Lineweaver, C. et al. 1994, ApJ, in press
- Sachs, R.K. & Wolfe, A.M. 1967, ApJ, 147, 73
- Scaramella, R. & Vittorio, N. 1993, MNRAS, 263, L17
- Seljak, U. & Bertschinger, E. 1993, ApJ, 417, L9
- Smoot, G.F. et al. 1992, ApJ, 396, L1
- Torres, S. 1994a, ApJ, 423, L9
- Torres, S. 1994b, "4th UN/ESA Workshop on Basic Space Sciences", eds. H. Haubold et al., in press
- Torres, S., Cayón, L., Martínez-González, E. & Sanz, J.L. 1994, submitted to MNRAS
- White, M., Scott, D. and Silk, J. 1994, ARA&A, in press

Wright, E.L., Smoot, G.F., Kogut, A., Hinshaw, G., Tenorio, L., Lineweaver, C., Bennett,
C.L. & Lubin, P.M. 1994a, ApJ, 420, 1

Wright, E.L. et al. 1994b, ApJ, 436, in press

Fig. 1a.— COBE/DMR 2 years maps at 31, 53 and 90 GHz showing the spots found at $|\nu| > 1$.

Fig. 1b.— COBE/DMR 2 years maps at 31, 53 and 90 GHz showing the spots found at $|\nu| > 2$.

Fig. 2.— χ^2 distribution for a 1000 realizations of noise (solid line) and of Harrison-Zeldovich power spectrum fluctuations with $Q_{rms-PS} = 15$ (dotted line), 27 (dashed line) μK , as compared with the first plus second year COBE/DMR data, by analysing the number of spots that appear at several thresholds.

Fig. 3a.— Distribution of the area of the spots observed above/below level $1/-1$ (solid/dashed line) in 1000 noise realizations.

Fig. 3b.— Distribution of the signal-to-noise of the spots observed above/below level 1/-1 (solid/ dashed line) in 1000 noise realizations.

1990+1991

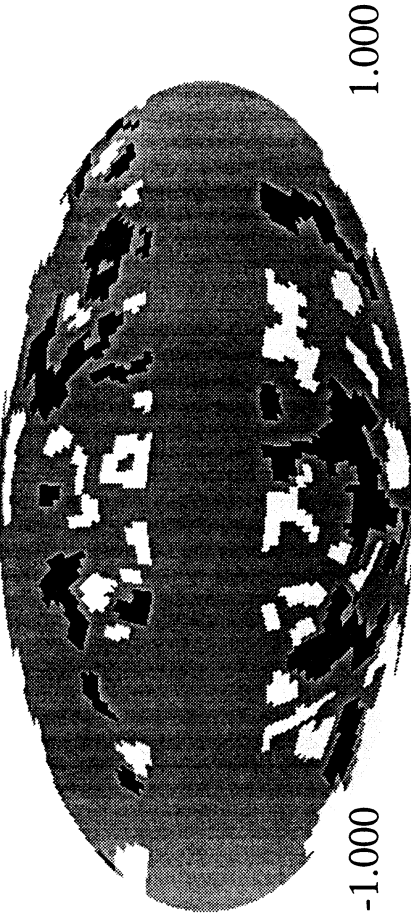
31 GHz



53 GHz

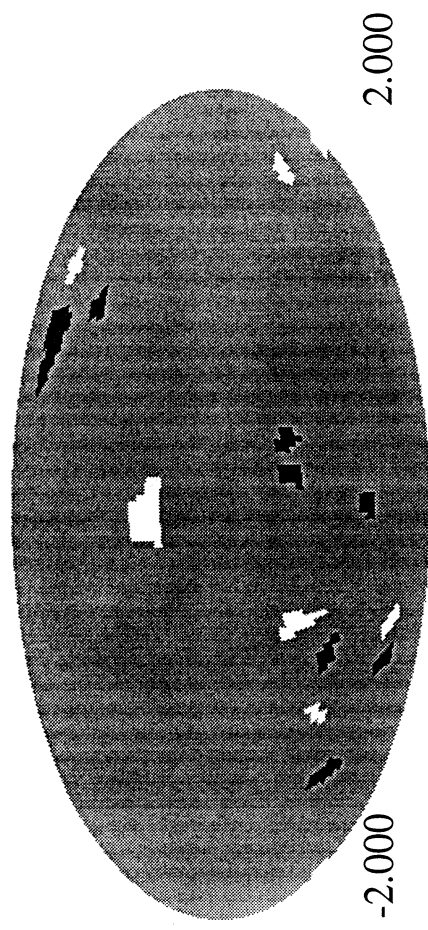


90 GHz

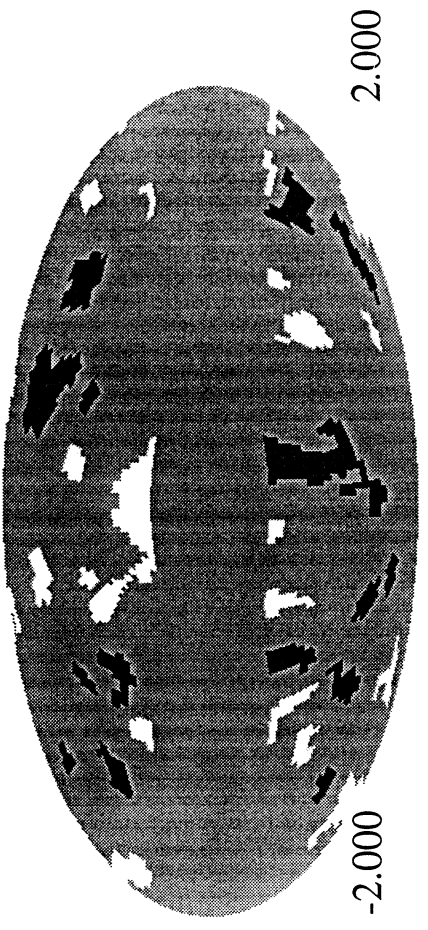


1990+1991

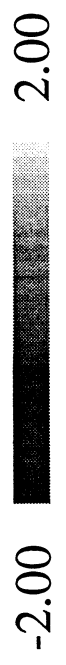
31 GHz



53 GHz



90 GHz



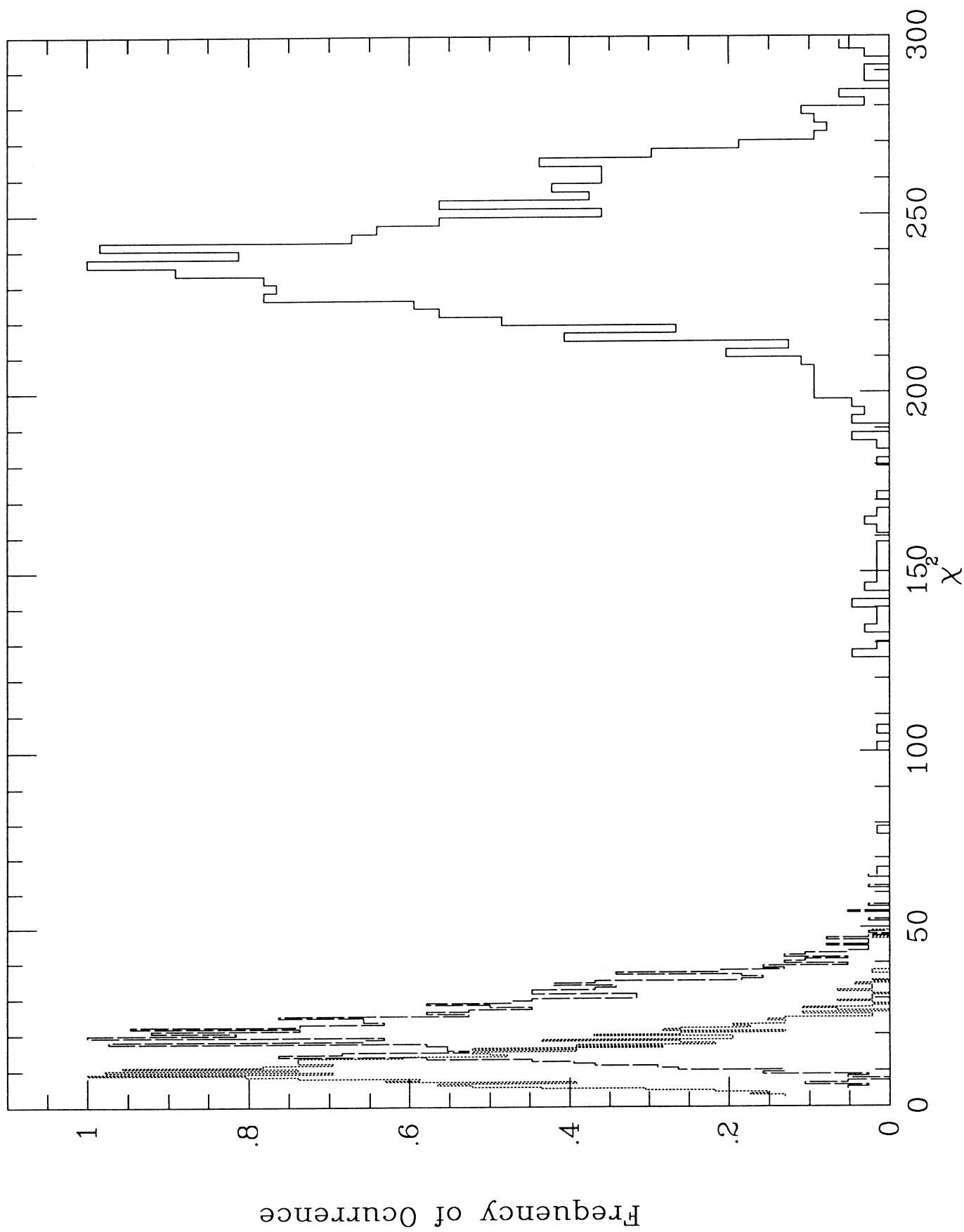


Fig. 2.

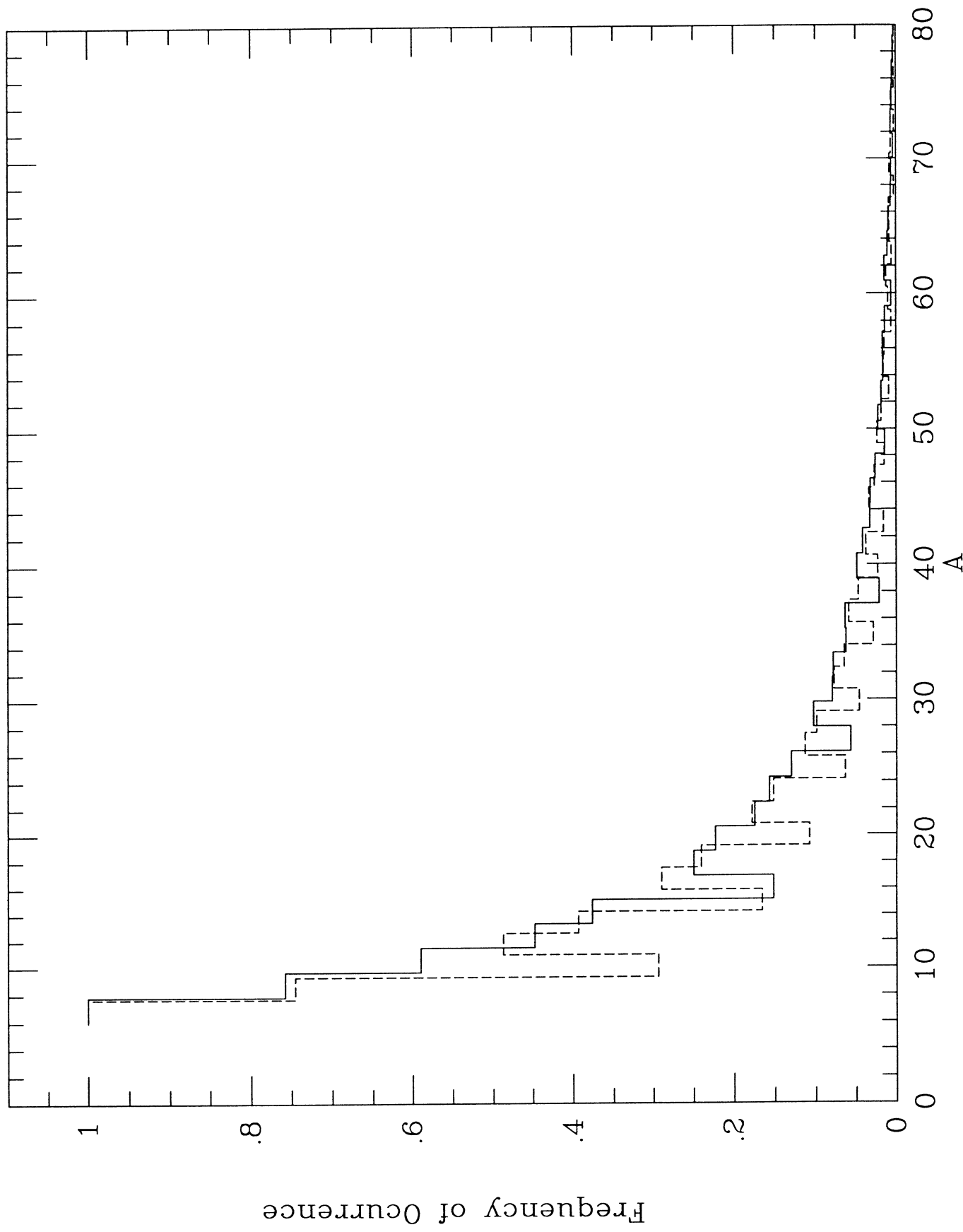


Fig. 3a.

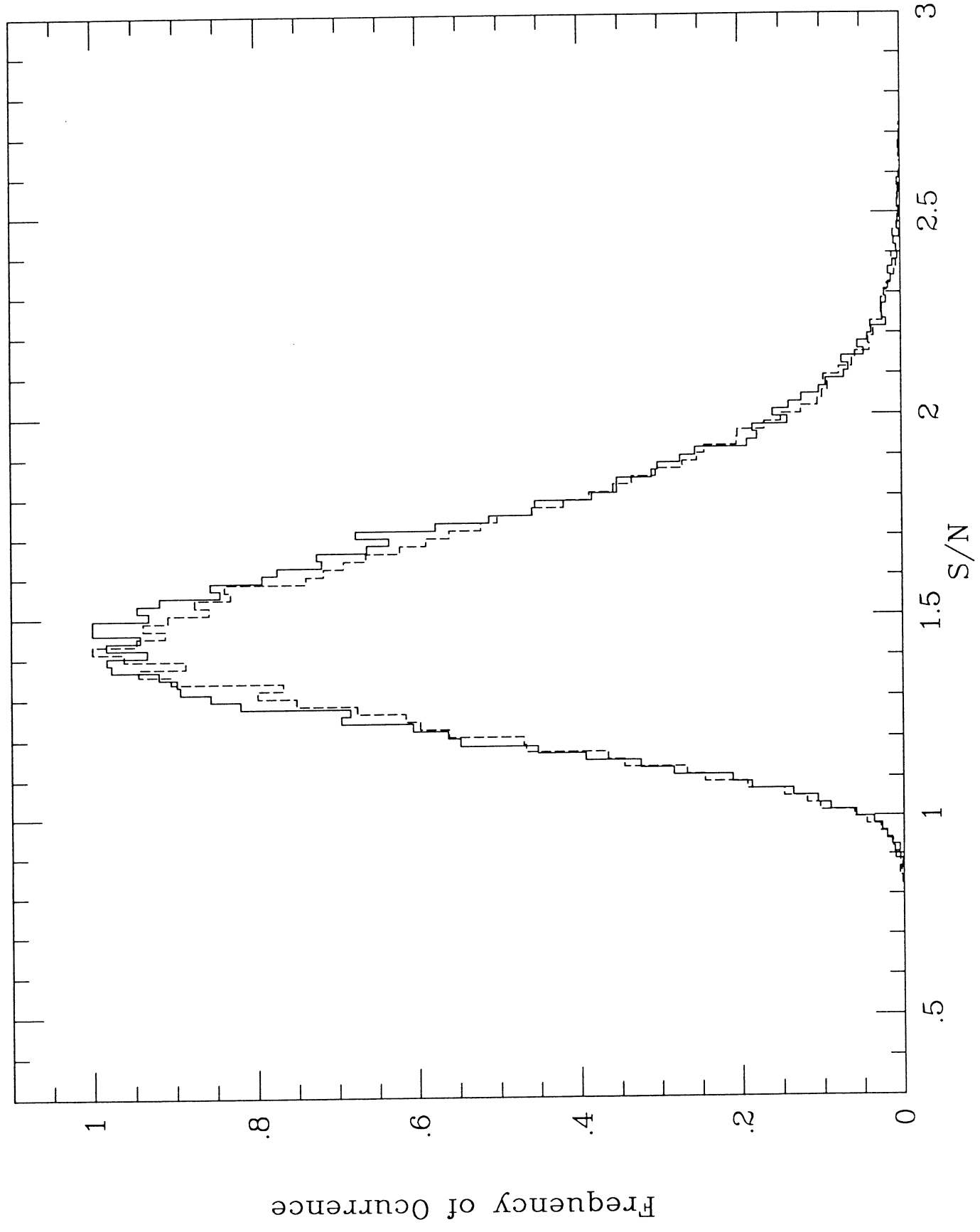


Fig. 3b.